Combined Search for Lorentz Violation in Short-Range Gravity

Cheng-Gang Shao, Yu-Jie Tan, Wen-Hai Tan, Shan-Qing Yang, and Jun Luo*
MOE Key Laboratory of Fundamental Physical Quantities Measurements, School of Physics, Huazhong University of Science and Technology, Wuhan 430074, People's Republic of China

Michael Edmund Tobar†
School of Physics, University of Western Australia, Crawley, Western Australia 6009, Australia

Quentin G. Bailey
Physics Department, Embry-Riddle Aeronautical University, Prescott, Arizona 86301, USA

J. C. Long,‡ E. Weisman, Rui Xu, and V. Alan Kostelecký§
Physics Department, Indiana University, Bloomington, Indiana 47405, USA

(Received 13 March 2016; revised manuscript received 29 May 2016; published 10 August 2016)

Short-range experiments testing the gravitational inverse-square law at the submillimeter scale offer uniquely sensitive probes of Lorentz invariance. A combined analysis of results from the short-range gravity experiments HUST-2015, HUST-2011, IU-2012, and IU-2002 permits the first independent measurements of the 14 nonrelativistic coefficients for Lorentz violation in the pure-gravity sector at the level of 10^{-9} m^2, improving by an order of magnitude the sensitivity to numerous types of Lorentz violation involving quadratic curvature derivatives and curvature couplings.

DOI: 10.1103/PhysRevLett.117.071102

General relativity offers an impressive description of gravity at the classical level. A key ingredient in its construction is local Lorentz invariance, which insures rotation and boost symmetry in a freely falling frame. However, achieving a consistent unification of gravity with quantum physics may require modifications of the foundations of general relativity. These modifications could induce observable violations of Lorentz invariance, arising in an underlying unified theory such as strings [1]. Experimental tests of Lorentz symmetry in gravity therefore have the potential to offer insight about the structure of physics beyond general relativity [2,3].

One interesting option for investigating Lorentz violation in pure gravity is offered by short-range experiments at the submillimeter scale [4]. Effective field theory for Lorentz violation in gravity [5] provides a generic and model-independent approach to studying possible experimental signals of Lorentz violation. Applying this method reveals that quadratic curvature derivatives and quadratic curvature couplings can produce novel signals in experiments on short-range gravity [6]. Most of these couplings remain experimentally unexplored and have *a priori* unknown sizes, with even comparatively large Lorentz violation remaining viable in certain "countershaded" models [7], so direct searches without preconceived notions of sensitivity are essential.

Short-range experiments at Indiana University (IU) [8] and Huazhong University of Science and Technology (HUST) [9] have achieved sensitivities at the level of 10^{-7} to 10^{-8} m^2 to individual coefficients controlling these types of gravitational local Lorentz violation. However, any one short-range experiment measures only nine signal components, which is insufficient to constrain simultaneously all the predicted effects. In this work, we present a combined analysis of results from tests of short-range gravity based on four different experimental designs performed at HUST (HUST-2015 [10] and HUST-2011 [9]) and at IU (IU-2012 and IU-2002 [8]). Our analysis yields the first independent measures of all 14 accessible coefficients for Lorentz violation, consistent with no effect at the level of 10^{-9} m^2.

The Lorentz-violating quadratic curvature derivatives and couplings produce a perturbative correction to the Newton gravitational potential between two test masses m_1, m_2 that is inverse cubic and varies with orientation and sidereal time T [6]. Its explicit form is

$$V_{\mathrm{LV}}(\vec{r}) = -G_N \frac{m_1 m_2}{|\vec{r}|^3} \bar{k}(\hat{r}, T), \tag{1}$$

where the vector $\vec{r} = \vec{x}_1 - \vec{x}_2$ separates m_1 and m_2, and

$$\bar{k} = \frac{3}{2}(\bar{k}_{\mathrm{eff}})_{jkjk} - 9(\bar{k}_{\mathrm{eff}})_{jkll}\hat{r}^j\hat{r}^k + \frac{15}{2}(\bar{k}_{\mathrm{eff}})_{jklm}\hat{r}^j\hat{r}^k\hat{r}^l\hat{r}^m \tag{2}$$

involves the projection $\hat{r}^j$ of the unit vector along $\vec{r}$ in the jth direction. The nonrelativistic coefficients $(\bar{k}_{\mathrm{eff}})_{jklm}$ for Lorentz violation have dimensions of squared length and are totally symmetric, thus containing 15 independent degrees of freedom. However, the rotation invariant $(\bar{k}_{\mathrm{eff}})_{jkjk}$ produces only a contact correction to the usual

Newton force, so only 14 of them are independently measurable in short-range experiments.

The coefficients $(\bar{k}_{\rm eff})_{jklm}$ take different forms in different inertial frames, so a canonical Sun-centered celestial-equatorial frame [2,11] is conventionally adopted to report experimental results, with the Z axis along the direction of Earth's rotation and the X axis pointing to the vernal equinox. The coefficients can be taken constant in this frame [12], but the rotation of Earth implies that the coefficients in a laboratory frame change with time and therefore produce sidereal signals in experimental data [13]. Neglecting Earth's boost $\beta_\oplus \simeq 10^{-4}$, the conversion from the Sun-centered frame (X, Y, Z) to a laboratory frame (x, y, z) with the x axis pointing to local south and the z axis to the zenith can be implemented by the time-dependent rotation

$$R^{jJ} = \begin{pmatrix} \cos\chi\cos\omega_\oplus T & \cos\chi\sin\omega_\oplus T & -\sin\chi \\ -\sin\omega_\oplus T & \cos\omega_\oplus T & 0 \\ \sin\chi\cos\omega_\oplus T & \sin\chi\sin\omega_\oplus T & \cos\chi \end{pmatrix}, \quad (3)$$

where $\omega_\oplus \simeq 2\pi/(23\ \text{h}\ 56\ \text{min})$ is the sidereal frequency. The laboratory colatitude χ is $\chi \simeq 1.038$ rad for HUST-2015 and HUST-2011, $\chi \simeq 0.887$ rad for IU-2012, and $\chi \simeq 0.872$ rad for IU-2002. The relation between the laboratory coefficients $(\bar{k}_{\rm eff})_{jklm}$ and the coefficients $(\bar{k}_{\rm eff})_{JKLM}$ in the Sun-centered frame is therefore

$$(\bar{k}_{\rm eff})_{jklm} = R^{jJ}R^{kK}R^{lL}R^{mM}(\bar{k}_{\rm eff})_{JKLM}. \quad (4)$$

It follows that the time oscillations of the inverse-cube potential (1) contain harmonic frequencies up to $4\omega_\oplus$.

Most experimental tests of the gravitational inverse-square law adopt a planar test-mass geometry to reduce conventional effects from Newton gravity. The Lorentz-violating force between two parallel plates can be calculated by numerical integration. Since only four harmonic frequencies appear, the signal from any one short-range experiment can contain at most nine Fourier components, including the dc response. Two or more experiments are therefore required to measure simultaneously all 14 independent Lorentz-violating degrees of freedom. Here, we achieve this using data from the recent experiment HUST-2015 [10] and from the earlier experiments IU-2012 [8], HUST-2011 [9], and IU-2002 [14]. Since the relevant methodologies for the latter three are described in detail elsewhere [8,9,14–16], we focus here on the corresponding analysis for HUST-2015.

The basic design and the operation of the experiment HUST-2015 are described in Ref. [10]. A bilaterally symmetric I-shaped pendulum is suspended next to an attractor disk with eightfold symmetry. The pendulum contains two pure-tungsten test masses, together with two additional tungsten pieces designed to compensate the Newton gravitational force at the signal frequency. The attractor disk consists of eight tungsten source masses and eight compensation masses. The centers of the attractor disk and the torsion pendulum are aligned, and the distance between the surfaces of the test and source masses is maintained at 295 μm. The pendulum twist is controlled using a feedback technique, by applying differential voltages to the two capacitive actuators on the pendulum. In the presence of Lorentz violation, rotating the attractor disk generates a torque. The signal and disturbance frequencies are well separated, so a high measurement resolution can be achieved. The apparatus is designed to produce approximate null measurements by double compensating for both the test and the source masses. When the attractor disk rotates at frequency $f_0 = 2\pi/(3846.12\ \text{s})$, the nominal signal torque oscillates at frequency $8f_0$. The torque is maximal when the source and test masses are face to face and minimal when they are offset. However, the Lorentz-violating force between two finite flat plates is dominated by edge effects [9], so the Lorentz-violating torque oscillates primarily at the frequency $16f_0$ and is an order of magnitude larger than the signal at $8f_0$. The resolution of the pendulum is calibrated gravitationally by rotating a nearby copper cylinder at frequency $f_c = 2\pi/(400\ \text{s})$, chosen to be close to $8f_0 \simeq 2\pi/(481\ \text{s})$ but sufficiently offset to be readily distinguished from it.

Data were acquired from December of 2014 to August of 2015, during a period of over 2000 hours. To extract the signal, the recorded data were separated into slices according to the modulation period, $\Delta T = 3846.12$ s. For each slice, the Lorentz-violating torque $\tau_{\rm LV}$ was extracted by fitting the measured torque $\tau^z(T)$ as

$$\tau^z(T) = \tau_{\rm LV}(T)\cos(32\pi f_0 T + \varphi), \quad (5)$$

where the initial phase φ is set by the operation of the experiment. We take $\tau_{\rm LV}(T)$ as approximately constant in each data slice because $\omega_\oplus \Delta T \ll 1$ and so any sidereal variation within each ΔT is negligible. The upper panel of Fig. 1 displays the extracted torque $\tau_{\rm LV}$ as a function of time. Each point represents the mean of the measurement in

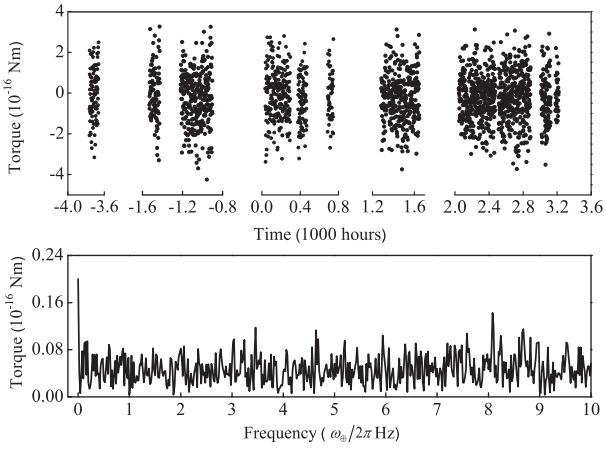

FIG. 1. HUST-2015 data at $16f_0$ and Fourier transform.

TABLE I. Fourier amplitudes (2σ, units 10^{-16} N m for HUST and 10^{-16} N for IU).

Mode	HUST-2015	HUST-2011	IU-2012	IU-2002
C_0	-0.20 ± 2.40	-0.22 ± 1.90	-31 ± 120	12 ± 203
C_1	0.00 ± 0.08	0.13 ± 0.44	-77 ± 170	34 ± 123
S_1	-0.01 ± 0.08	-0.40 ± 0.45	-7 ± 154	-98 ± 242
C_2	-0.01 ± 0.08	-0.04 ± 0.45	16 ± 154	-66 ± 278
S_2	-0.09 ± 0.08	0.20 ± 0.45	-151 ± 167	-52 ± 139
C_3	0.01 ± 0.08	-0.30 ± 0.45	-164 ± 144	207 ± 141
S_3	-0.06 ± 0.08	0.25 ± 0.45	181 ± 176	-144 ± 216
C_4	0.04 ± 0.08	-0.06 ± 0.45	2 ± 142	26 ± 223
S_4	-0.03 ± 0.08	0.05 ± 0.45	-10 ± 165	74 ± 159

ΔT without error, which is dominated by statistical uncertainty. In the Sun-centered frame, the time origin $T = 0$ is defined as the vernal equinox 2000. For the analysis, it suffices to use a convenient shifted time $T_\oplus$ with origin set when local east coincides with the Y axis of the Sun-centered frame [11]. The lower panel of Fig. 1 shows the Fourier spectrum of the torque.

Using Eqs. (1) and (2), the Lorentz-violating acceleration at any position due to the source can be obtained via an integral over the geometry of the source mass. The Lorentz-violating signal between the source and test masses can then be extracted by a further integration over the geometry of the test mass. The data are fitted to a Fourier series in the sidereal time $T_\oplus$,

TABLE II. Independent coefficient values (2σ, units 10^{-9} m^2) obtained by combining HUST and IU data [8–10].

Coefficient	Measurement
$(\bar{k}_{\rm eff})_{XXXX}$	6.4 ± 32.9
$(\bar{k}_{\rm eff})_{XXXY}$	0.0 ± 8.1
$(\bar{k}_{\rm eff})_{XXXZ}$	-2.0 ± 2.6
$(\bar{k}_{\rm eff})_{XXYY}$	-0.9 ± 10.9
$(\bar{k}_{\rm eff})_{XXYZ}$	1.1 ± 1.2
$(\bar{k}_{\rm eff})_{XXZZ}$	-2.6 ± 17.1
$(\bar{k}_{\rm eff})_{XYYY}$	3.9 ± 8.1
$(\bar{k}_{\rm eff})_{XYYZ}$	-0.6 ± 1.2
$(\bar{k}_{\rm eff})_{XYZZ}$	-1.0 ± 1.0
$(\bar{k}_{\rm eff})_{XZZZ}$	-8.1 ± 10.3
$(\bar{k}_{\rm eff})_{YYYY}$	7.0 ± 32.9
$(\bar{k}_{\rm eff})_{YYYZ}$	0.3 ± 2.6
$(\bar{k}_{\rm eff})_{YYZZ}$	-2.5 ± 17.1
$(\bar{k}_{\rm eff})_{YZZZ}$	3.6 ± 10.2

$$\tau_{\rm LV}(T_\oplus) = C_0 + \sum_{m=1}^{4} \frac{\sin(m\omega_\oplus \Delta T/2)}{m\omega_\oplus \Delta T/2} \times [C_m \cos(m\omega_\oplus T_\oplus) + S_m \sin(m\omega_\oplus T_\oplus)]. \quad (6)$$

In this expression, the Fourier amplitudes are functions of the test-mass and source-mass geometry, the laboratory colatitude, and the coefficients $(\bar{k}_{\rm eff})_{JKLM}$ in the Sun-centered frame. For a sinusoidal signal at frequency

TABLE III. Constraints (2σ, units 10^{-9} m^2) on 59 independent coefficients $(k_1^{(6)})_{\alpha\beta\gamma\delta\kappa\lambda}$ taken one at a time.

Coefficient	Measurement	Coefficient	Measurement	Coefficient	Measurement
$(\bar{k}_1^{(6)})_{XTXTXX}$	-0.8 ± 6.3	$(\bar{k}_1^{(6)})_{XYXYYY}$	-0.2 ± 36.3	$(\bar{k}_1^{(6)})_{XZYZZZ}$	-3.2 ± 2.9
$(\bar{k}_1^{(6)})_{XTXTXY}$	1.6 ± 2.3	$(\bar{k}_1^{(6)})_{XYXYYZ}$	1.4 ± 1.8	$(\bar{k}_1^{(6)})_{YTYTXX}$	0.1 ± 9.9
$(\bar{k}_1^{(6)})_{XTXTXZ}$	1.2 ± 1.2	$(\bar{k}_1^{(6)})_{XYXYZZ}$	-1.8 ± 7.6	$(\bar{k}_1^{(6)})_{YTYTXY}$	1.3 ± 2.3
$(\bar{k}_1^{(6)})_{XTXTYY}$	-0.4 ± 27.6	$(\bar{k}_1^{(6)})_{XYXZXX}$	3.2 ± 3.7	$(\bar{k}_1^{(6)})_{YTYTXZ}$	1.4 ± 1.5
$(\bar{k}_1^{(6)})_{XTXTYZ}$	-1.2 ± 1.5	$(\bar{k}_1^{(6)})_{XYXZXY}$	0.1 ± 1.5	$(\bar{k}_1^{(6)})_{YTYTYY}$	-3.1 ± 11.8
$(\bar{k}_1^{(6)})_{XTXTZZ}$	2.2 ± 12.4	$(\bar{k}_1^{(6)})_{XYXZXZ}$	-1.5 ± 1.5	$(\bar{k}_1^{(6)})_{YTYTYZ}$	-0.5 ± 1.2
$(\bar{k}_1^{(6)})_{XTYTXX}$	0.0 ± 8.1	$(\bar{k}_1^{(6)})_{XYXZYY}$	-1.0 ± 1.5	$(\bar{k}_1^{(6)})_{YTYTZZ}$	2.8 ± 14.1
$(\bar{k}_1^{(6)})_{XTYTXY}$	-0.1 ± 6.9	$(\bar{k}_1^{(6)})_{XYXZYZ}$	0.8 ± 4.5	$(\bar{k}_1^{(6)})_{YTZTXX}$	-3.2 ± 3.7
$(\bar{k}_1^{(6)})_{XTYTXZ}$	-1.6 ± 1.8	$(\bar{k}_1^{(6)})_{XYXZZZ}$	-1.4 ± 1.8	$(\bar{k}_1^{(6)})_{YTZTXY}$	0.8 ± 1.8
$(\bar{k}_1^{(6)})_{XTYTYY}$	-4.0 ± 8.1	$(\bar{k}_1^{(6)})_{XYYZYY}$	1.7 ± 3.7	$(\bar{k}_1^{(6)})_{YTZTXZ}$	1.6 ± 1.5
$(\bar{k}_1^{(6)})_{XTYTYZ}$	0.8 ± 1.8	$(\bar{k}_1^{(6)})_{XYYZYZ}$	1.5 ± 1.5	$(\bar{k}_1^{(6)})_{YTZTYY}$	-0.3 ± 2.6
$(\bar{k}_1^{(6)})_{XTYTZZ}$	3.2 ± 2.9	$(\bar{k}_1^{(6)})_{XYYZZZ}$	-1.4 ± 2.6	$(\bar{k}_1^{(6)})_{YTZTZZ}$	-3.6 ± 10.2
$(\bar{k}_1^{(6)})_{XTZTXX}$	2.0 ± 2.6	$(\bar{k}_1^{(6)})_{XZXZXX}$	-0.5 ± 27.6	$(\bar{k}_1^{(6)})_{YZYZYY}$	-0.5 ± 27.6
$(\bar{k}_1^{(6)})_{XTZTXY}$	-1.6 ± 1.8	$(\bar{k}_1^{(6)})_{XZXZXY}$	-2.0 ± 5.7	$(\bar{k}_1^{(6)})_{YZYZYZ}$	-3.2 ± 3.7
$(\bar{k}_1^{(6)})_{XTZTXZ}$	0.1 ± 9.1	$(\bar{k}_1^{(6)})_{XZXZXZ}$	1.7 ± 3.7	$(\bar{k}_1^{(6)})_{ZTZTXX}$	0.2 ± 9.8
$(\bar{k}_1^{(6)})_{XTZTYY}$	1.7 ± 3.7	$(\bar{k}_1^{(6)})_{XZXZYY}$	-1.7 ± 6.5	$(\bar{k}_1^{(6)})_{ZTZTXY}$	1.4 ± 1.4
$(\bar{k}_1^{(6)})_{XTZTYZ}$	1.6 ± 1.5	$(\bar{k}_1^{(6)})_{XZXZYZ}$	1.0 ± 1.5	$(\bar{k}_1^{(6)})_{ZTZTXZ}$	2.2 ± 2.0
$(\bar{k}_1^{(6)})_{XTZTZZ}$	8.1 ± 10.3	$(\bar{k}_1^{(6)})_{XZXZZZ}$	-0.2 ± 36.3	$(\bar{k}_1^{(6)})_{ZTZTYZ}$	-1.3 ± 2.0
$(\bar{k}_1^{(6)})_{XYXYXY}$	3.2 ± 2.9	$(\bar{k}_1^{(6)})_{XZYZYY}$	2.0 ± 5.7	$(\bar{k}_1^{(6)})_{ZTZTZZ}$	0.6 ± 10.9
$(\bar{k}_1^{(6)})_{XYXYXZ}$	-1.4 ± 2.6	$(\bar{k}_1^{(6)})_{XZYZYZ}$	0.1 ± 1.5		

$m\omega_\oplus$, the data average over ΔT intervals leads to an attenuation of the amplitude by the factor $1-\sin(m\omega_\oplus \Delta T/2)/m\omega_\oplus \Delta T/2$, which is approximately 0.

Table I displays the measurements of the nine signal Fourier components. The results for the HUST-2015 experiment extracted from the fit (6) are shown in the second column. The third column contains the results from the HUST-2011 analysis [9], while the fourth and fifth columns show those from the IU-2012 and IU-2002 analyses. Note that the HUST data are torque amplitudes while the IU data are force amplitudes, with similar relative errors.

The HUST-2015 apparatus was designed to detect a non-Newton force at $8f_0$, for which the Newton force is compensated by the design. However, the present work uses the data at frequency $16f_0$, for which the Newton force is imperfectly compensated. The errors arise from uncertainties in the dimensions and locations of the test and source masses. This leads to a comparatively large systematic error that is restricted to the dc Fourier component C_0 of the $16f_0$ signal and can be seen in the lower panel of Fig. 1. In general, experiments searching for sidereal signals are susceptible to systematic errors arising from mundane diurnal variations. For HUST-2015, the dominant contribution of this type is due to temperature fluctuations. This affects the torque in two main ways. First, it changes the dimensions and relative positions of the pendulum and the attractor, which leads to a variation of the amplitude of the $16f_0$ Newtonian torque. The temperature is recorded synchronously throughout the data collection. For a typical temperature data set taken over a period of 9.5 days in March of 2015, only diurnal and semidiurnal variations with amplitudes of 3.8 ± 1.3 and 4.9 ± 0.7 mK are evident. The largest variation of the geometric parameters is the relative height between the pendulum and the attractor, which is about 0.04 μm, resulting in a negligible variation of $< 0.06 \times 10^{-16}$ N m in the amplitude of the $16f_0$ Newtonian torque. Second, the temperature fluctuation changes the equilibrium positon of the torsion balance. This leads directly to a torque variation, with a temperature-to-torque coefficient of $(1.1 \pm 0.2) \times 10^{-12}$ Nm/K. However, the relevant concern is the diurnal and harmonic variations of the amplitude of the $16f_0$ signal, which are $< (2 \pm 2)$ μK, resulting in a torque noise of $< 0.06 \times 10^{-16}$ N m at the 2σ level. This is included in the statistical errors listed in Table I. In effect, the total noise is stable in the frequency band relevant to the Lorentz-violating signal, so the

TABLE IV. Constraints (2σ, units 10^{-9} m^2) on 72 independent coefficients $(k_2^{(6)})_{\alpha\beta\gamma\delta\kappa\lambda\mu\nu}$ taken one at a time.

Coefficient	Measurement	Coefficient	Measurement	Coefficient	Measurement
$(\bar{k}_2^{(6)})_{XTXTXTXT}$	0.7 ± 3.0	$(\bar{k}_2^{(6)})_{XTZTXYXY}$	-0.2 ± 0.3	$(\bar{k}_2^{(6)})_{ZTZTZTZT}$	0.6 ± 4.3
$(\bar{k}_2^{(6)})_{XTXTXTYT}$	0.0 ± 1.0	$(\bar{k}_2^{(6)})_{XTZTXYXZ}$	-0.2 ± 0.2	$(\bar{k}_2^{(6)})_{ZTZTXYXZ}$	0.5 ± 1.3
$(\bar{k}_2^{(6)})_{XTXTXTZT}$	-0.2 ± 0.3	$(\bar{k}_2^{(6)})_{XTZTXYYZ}$	0.0 ± 1.1	$(\bar{k}_2^{(6)})_{ZTZTXYYZ}$	1.0 ± 1.3
$(\bar{k}_2^{(6)})_{XTXTXYXY}$	0.3 ± 1.4	$(\bar{k}_2^{(6)})_{XTZTXZXZ}$	-0.3 ± 0.3	$(\bar{k}_2^{(6)})_{ZTZTXZXZ}$	0.3 ± 2.1
$(\bar{k}_2^{(6)})_{XTXTXYXZ}$	0.4 ± 0.5	$(\bar{k}_2^{(6)})_{XTZTXZYZ}$	0.2 ± 0.2	$(\bar{k}_2^{(6)})_{ZTZTXZYZ}$	-0.4 ± 0.4
$(\bar{k}_2^{(6)})_{XTXTXYYZ}$	0.2 ± 0.3	$(\bar{k}_2^{(6)})_{XTZTYTYT}$	-0.2 ± 0.5	$(\bar{k}_2^{(6)})_{XYXYXYXY}$	0.4 ± 2.6
$(\bar{k}_2^{(6)})_{XTXTXZXZ}$	0.4 ± 1.5	$(\bar{k}_2^{(6)})_{XTZTYTZT}$	-0.2 ± 0.2	$(\bar{k}_2^{(6)})_{XYXYXYXZ}$	0.2 ± 0.3
$(\bar{k}_2^{(6)})_{XTXTXZYZ}$	0.0 ± 1.0	$(\bar{k}_2^{(6)})_{XTZTYZYZ}$	-0.3 ± 0.4	$(\bar{k}_2^{(6)})_{XYXYXYYZ}$	0.2 ± 0.3
$(\bar{k}_2^{(6)})_{XTXTYTYT}$	0.1 ± 3.5	$(\bar{k}_2^{(6)})_{XTZTZTZT}$	-1.0 ± 1.3	$(\bar{k}_2^{(6)})_{XYXYXZXZ}$	0.4 ± 2.1
$(\bar{k}_2^{(6)})_{XTXTYTZT}$	0.4 ± 0.5	$(\bar{k}_2^{(6)})_{YTYTXYXY}$	0.3 ± 1.4	$(\bar{k}_2^{(6)})_{XYXYXZYZ}$	0.2 ± 0.7
$(\bar{k}_2^{(6)})_{XTXTYZYZ}$	0.1 ± 3.5	$(\bar{k}_2^{(6)})_{YTYTXYXZ}$	0.0 ± 0.3	$(\bar{k}_2^{(6)})_{XYXYYZYZ}$	0.5 ± 2.1
$(\bar{k}_2^{(6)})_{XTXTZTZT}$	0.0 ± 4.5	$(\bar{k}_2^{(6)})_{YTYTXYYZ}$	0.2 ± 0.5	$(\bar{k}_2^{(6)})_{XYXZXYXZ}$	-0.5 ± 1.7
$(\bar{k}_2^{(6)})_{XTYTXTYT}$	0.0 ± 1.7	$(\bar{k}_2^{(6)})_{YTYTXZXZ}$	0.1 ± 3.5	$(\bar{k}_2^{(6)})_{XYXZXZXZ}$	0.4 ± 0.4
$(\bar{k}_2^{(6)})_{XTYTXTZT}$	0.2 ± 0.2	$(\bar{k}_2^{(6)})_{YTYTXZYZ}$	0.5 ± 1.0	$(\bar{k}_2^{(6)})_{XYXZYZYZ}$	0.1 ± 0.3
$(\bar{k}_2^{(6)})_{XTYTXYXY}$	0.2 ± 0.7	$(\bar{k}_2^{(6)})_{YTYTYTYT}$	0.8 ± 3.0	$(\bar{k}_2^{(6)})_{XYYZXYXZ}$	0.2 ± 0.2
$(\bar{k}_2^{(6)})_{XTYTXYXZ}$	-0.1 ± 0.2	$(\bar{k}_2^{(6)})_{YTYTYTZT}$	0.0 ± 0.3	$(\bar{k}_2^{(6)})_{XYYZXYYZ}$	-0.3 ± 1.4
$(\bar{k}_2^{(6)})_{XTYTXYYZ}$	-0.2 ± 0.2	$(\bar{k}_2^{(6)})_{YTYTYZYZ}$	0.5 ± 1.7	$(\bar{k}_2^{(6)})_{XYYZXZYZ}$	-0.2 ± 0.2
$(\bar{k}_2^{(6)})_{XTYTXZXZ}$	-0.3 ± 0.3	$(\bar{k}_2^{(6)})_{YTZTXYXY}$	0.2 ± 0.3	$(\bar{k}_2^{(6)})_{XYYZYZYZ}$	0.3 ± 0.4
$(\bar{k}_2^{(6)})_{XTYTXZYZ}$	0.0 ± 0.9	$(\bar{k}_2^{(6)})_{YTZTXYYZ}$	0.2 ± 0.2	$(\bar{k}_2^{(6)})_{XZXZXYYZ}$	0.3 ± 0.3
$(\bar{k}_2^{(6)})_{XTYTYTYT}$	0.5 ± 1.0	$(\bar{k}_2^{(6)})_{YTZTXZXZ}$	0.4 ± 0.4	$(\bar{k}_2^{(6)})_{XZXZXZXZ}$	0.0 ± 2.4
$(\bar{k}_2^{(6)})_{XTYTYTZT}$	-0.1 ± 0.2	$(\bar{k}_2^{(6)})_{YTZTXZYZ}$	-0.1 ± 0.2	$(\bar{k}_2^{(6)})_{XZXZXZYZ}$	-0.3 ± 0.3
$(\bar{k}_2^{(6)})_{XTYTYZYZ}$	-0.3 ± 0.3	$(\bar{k}_2^{(6)})_{YTZTYZYZ}$	0.1 ± 0.3	$(\bar{k}_2^{(6)})_{XZYZXYXZ}$	-0.1 ± 0.2
$(\bar{k}_2^{(6)})_{XTYTZTZT}$	-0.4 ± 0.4	$(\bar{k}_2^{(6)})_{YTZTZTZT}$	0.5 ± 1.3	$(\bar{k}_2^{(6)})_{XZYZXZYZ}$	-0.2 ± 1.1
$(\bar{k}_2^{(6)})_{XTZTXTZT}$	0.0 ± 2.3	$(\bar{k}_2^{(6)})_{ZTZTYZYZ}$	0.6 ± 2.9	$(\bar{k}_2^{(6)})_{XZYZYZYZ}$	-0.3 ± 0.3

uncertainties for the modes C_m and S_m are the same size and dominated by statistics. The net results of this error budgeting are shown in Table I.

Simultaneous analysis of all these data yields independent measurements of 14 accessible degrees of freedom. Table II displays these measurements in the Sun-centered frame. A convenient choice of the 14 independent effective coefficients has been made, and the table lists them alphabetically by indices. The 14 independent effective coefficients $(\bar{k}_{\rm eff})_{JKLM}$ appearing in Table II are linear combinations of a subset of the fundamental coefficients $(k_1^{(6)})_{\alpha\beta\gamma\delta\kappa\lambda}$ and $(k_2^{(6)})_{\alpha\beta\gamma\delta\kappa\lambda\mu\nu}$ that govern quadratic curvature derivatives and couplings in Lorentz-violating gravity [6]. The relationship is

$$\begin{aligned}(\bar{k}_{\rm eff})_{JKLM} = &-2(\bar{k}_1^{(6)})_{T(JTKLM)} - 2(\bar{k}_1^{(6)})_{N(JKNLM)} \\ &- 2(\bar{k}_1^{(6)})_{NTNT(JK}\delta_{LM)} - (\bar{k}_1^{(6)})_{NPNP(JK}\delta_{LM)} \\ &+ 8(\bar{k}_2^{(6)})_{T(JTKTLTM)} + 8(\bar{k}_2^{(6)})_{N(JNKPLPM)} \\ &+ 16(\bar{k}_2^{(6)})_{T(JTKNLNM)}, \end{aligned} \tag{7}$$

where the symmetry indicated by the parentheses is on the spatial indices $JKLM$ only, and T is the temporal index. The parameter a used in Eq. (6) of Ref. [6] has been set to 0, which is possible without loss of generality [17]. Counting coefficients reveals that Eq. (7) involves 63 of the 126 independent degrees of freedom in $(k_1^{(6)})_{\alpha\beta\gamma\delta\kappa\lambda}$ and 78 of the 210 independent degrees of freedom in $(k_2^{(6)})_{\alpha\beta\gamma\delta\kappa\lambda\mu\nu}$. However, some of these are rotation invariants and hence cannot be detected via sidereal studies, implying that our analysis achieves sensitivity to 59 independent degrees of freedom in $(k_1^{(6)})_{\alpha\beta\gamma\delta\kappa\lambda}$ and 72 in $(k_2^{(6)})_{\alpha\beta\gamma\delta\kappa\lambda\mu\nu}$. Using Eq. (7), we can transform the 14 independent measurements given in Table II into limits on a conveniently chosen set of $59 + 72 = 131$ independent coefficients taken one at a time, following standard procedure in the field [2]. This procedure yields the measurements shown in Tables III and IV.

To summarize, a combined analysis of data from the short-range experiments HUST-2015, HUST-2011, IU-2012, and IU-2002 constrains simultaneously and independently 14 combinations of coefficients for Lorentz violation, consistent with no effect at the level of 10^{-9} m^2. This represents an improvement of an order of magnitude over previous experimental analyses, achieving sensitivity to 131 independent types of Lorentz-violating quadratic curvature derivatives and couplings. The results presented in this work complement recent limits obtained on 25 independent coefficients [18] from gravitational Čerenkov radiation and on 39 independent coefficients [17] from the gravitational-wave event GW150914 [19]. They also complement experimental searches for a Lorentz-violating inverse-square law [20–29].

This work was supported by the National Natural Science Foundation of China (Grants No. 11275075, No. 11325523, and No. 91436212) and 111 project (Grant No. B14030), the Australian Research Council Grant No. DP160100253, the United States National Science Foundation under Grants No. PHY-1207656 and No. PHY-1402890, the United States Department of Energy under Award No. DE-SC0010120, and the Indiana University Center for Spacetime Symmetries.

*junluo@sysu.edu.cn
†michael.tobar@uwa.edu.au
‡jcl@indiana.edu
§kostelec@indiana.edu

[1] V. A. Kostelecký and S. Samuel, Phys. Rev. D **39**, 683 (1989); V. A. Kostelecký and R. Potting, Nucl. Phys. **B359**, 545 (1991); Phys. Rev. D **51**, 3923 (1995).
[2] V. A. Kostelecký and N. Russell, Rev. Mod. Phys. **83**, 11 (2011).
[3] For reviews see, for example, J. D. Tasson, Rep. Prog. Phys. **77**, 062901 (2014); C. M. Will, Living Rev. Relativ. **17**, 4 (2014); R. Bluhm, Lect. Notes Phys. **702**, 191 (2006).
[4] For reviews see, for example, J. Murata and S. Tanaka, Classical Quantum Gravity **32**, 033001 (2015); J. Jaeckel and A. Ringwald, Annu. Rev. Nucl. Part. Sci. **60**, 405 (2010); E. G. Adelberger, J. H. Gundlach, B. R. Heckel, S. Hoedl, and S. Schlamminger, Prog. Part. Nucl. Phys. **62**, 102 (2009); E. Fischbach and C. Talmadge, *The Search for Non-Newtonian Gravity* (Springer-Verlag, Berlin, 1999).
[5] V. A. Kostelecký, Phys. Rev. D **69**, 105009 (2004).
[6] Q. G. Bailey, V. A. Kostelecký, and R. Xu, Phys. Rev. D **91**, 022006 (2015).
[7] V. A. Kostelecký and J. D. Tasson, Phys. Rev. Lett. **102**, 010402 (2009).
[8] J. C. Long and V. A. Kostelecký, Phys. Rev. D **91**, 092003 (2015).
[9] C.-G. Shao, Y.-J. Tan, W.-H. Tan, S.-Q. Yang, J. Luo, and M. E. Tobar, Phys. Rev. D **91**, 102007 (2015).
[10] W.-H. Tan, S.-Q. Yang, C.-G. Shao, J. Li, A.-B. Du, B.-F. Zhan, Q.-L. Wang, P.-S. Luo, L.-C. Tu, and J. Luo, Phys. Rev. Lett. **116**, 131101 (2016).
[11] R. Bluhm, V. A. Kostelecký, C. D. Lane, and N. Russell, Phys. Rev. D **68**, 125008 (2003); Phys. Rev. Lett. **88**, 090801 (2002); V. A. Kostelecký and M. Mewes, Phys. Rev. D **66**, 056005 (2002).
[12] D. Colladay and V. A. Kostelecký, Phys. Rev. D **55**, 6760 (1997); **58**, 116002 (1998).
[13] V. A. Kostelecký, Phys. Rev. Lett. **80**, 1818 (1998).
[14] J. C. Long, H. W. Chan, A. B. Churnside, E. A. Gulbis, M. C. M. Varney, and J. C. Price, Nature (London) **421**, 922 (2003).
[15] J. C. Long, H. W. Chan, A. B. Churnside, E. A. Gulbis, M. C. M. Varney, and J. C. Price, arXiv:hep-ph/0210004.
[16] H. Yan, E. A. Housworth, H. O. Meyer, G. Visser, E. Weisman, and J. C. Long, Classical Quantum Gravity **31**, 205007 (2014).

[17] V. A. Kostelecký and M. Mewes, Phys. Lett. B **757**, 510 (2016).
[18] V. A. Kostelecký and J. D. Tasson, Phys. Lett. B **749**, 551 (2015).
[19] B. P. Abbott *et al.* (LIGO Scientific Collaboration and Virgo Collaboration), Phys. Rev. Lett. **116**, 061102 (2016).
[20] Q. G. Bailey and V. A. Kostelecký, Phys. Rev. D **74**, 045001 (2006).
[21] J. B. R. Battat, J. F. Chandler, and C. W. Stubbs, Phys. Rev. Lett. **99**, 241103 (2007).
[22] H. Müller, S.-w. Chiow, S. Herrmann, S. Chu, and K.-Y. Chung, Phys. Rev. Lett. **100**, 031101 (2008).
[23] K.-Y. Chung, S.-w. Chiow, S. Herrmann, S. Chu, and H. Müller, Phys. Rev. D **80**, 016002 (2009).
[24] D. Bennett, V. Skavysh, and J. Long, in *CPT and Lorentz Symmetry V*, edited by V. A. Kostelecký (World Scientific, Singapore, 2011).
[25] L. Iorio, Classical Quantum Gravity **29**, 175007 (2012).
[26] Q. G. Bailey, R. D. Everett, and J. M. Overduin, Phys. Rev. D **88**, 102001 (2013).
[27] L. Shao, Phys. Rev. Lett. **112**, 111103 (2014); Phys. Rev. D **90**, 122009 (2014).
[28] A. Hees, Q. G. Bailey, C. Le Poncin-Lafitte, A. Bourgoin, A. Rivoldini, B. Lamine, F. Meynadier, C. Guerlin, and P. Wolf, Phys. Rev. D **92**, 064049 (2015).
[29] A. Bourgoin, A. Hees, S. Bouquillon, C. Le Poncin-Lafitte, G. Francou, and M.-C. Angonin, arXiv:1607.00294.